

Stable memory with unstable synapses

Lee Susman^{1,2,*}, Naama Brenner^{2,3}, and Omri Barak^{2,4}

¹*Interdisciplinary program in Applied Mathematics, Technion Israel Institute of Technology, Haifa, Israel*

²*Network Biology Research Laboratories, Technion Israel Institute of Technology, Haifa, Israel*

³*Faculty of Chemical Engineering, Technion Israel Institute of Technology, Haifa, Israel*

⁴*Rappaport Faculty of Medicine, Technion Israel Institute of Technology, Haifa, Israel*

*email: lee.susman@gmail.com

What is the physiological basis of long term memory? The current dogma in theoretical neuroscience attributes changes in synaptic efficacy to memory acquisition. This view implies that in the absence of learning, synaptic efficacies should be constant; in other words, stable memories correspond to stable connectivity patterns. However, an increasing body of experimental evidence points to significant, activity-independent dynamics in synaptic strengths. These fluctuations seem to be occurring continuously, without specific reference to a learning process, but with similar magnitude. Motivated by these observations, we explore the possibility of memory storage within a specific component of network connectivity, while individual connections fluctuate in time. We find a family of neural network models in which memory is acquired by means of biologically-inspired learning rules; the properties of these rules, in turn, determine the storing component in which memory can persist indefinitely. Memory representations manifest as time-varying attractors in neural state-space and support associative retrieval of learned information. Our results suggest a link between the properties of learning rules and those of network-level memory representations, which generates experimentally-testable predictions.

The ability to form and retain memories of past experience is fundamental to behavior, supporting adaptable responses and future planning [1]. These internal representations persist over extended durations and may be re-activated by appropriate retrieval cues [2]. Currently, it is widely accepted that synaptic connections between neurons play a central role in the physiological basis of long-term memory storage [3] (see [4, 5] for other possibilities). The process of learning, on its part, is understood as stimulus-driven neural activity sculpting network architecture, i.e. Hebbian plasticity [6].

If an internal memory-representation is stable over time, then one could assume that some properties of its underlying neural implementations also exhibit invariance over this period. However, at the level of single synapses, no such robustness exists (reviewed in [7, 8, 9, 10]). Over the past decade, several studies, both in vitro [11, 12] and in vivo [13, 14], suggest that synapses undergo significant spontaneous changes. These fluctuations are independent of neural activity, with magnitude estimated to be as large as that of directed, Hebbian, plasticity [12].

How, then, can memory traces remain stable over time? Various studies have proposed candidate invariant features, at different levels of organization of neural networks [7]. For single synapses, invariance may be implemented in a sub-set of the largest spines [14, 15]. Invariance may, instead, only emerge at the level of the connection between neurons, typically comprising several synapses. This allows individual synapses to fluctuate, under the constraint of stable overall connection strength between two cells [16, 17]. Higher up

the organizational hierarchy, invariant features may manifest only at the level of networks. This would allow individual connections to fluctuate, provided that some network properties remain invariant [9].

In this work, we rely on known properties of synaptic plasticity to suggest a natural segregation of synaptic modifications at the network level. Specifically, Spike Timing Dependent Plasticity (STDP) is a temporally asymmetric phenomenon [18]; we will show that such learning-rules correspond to particular connectivity structures encoding for memory traces. On the other hand, a mathematically consistent implementation of known homeostatic mechanisms leads to spontaneous synaptic fluctuations, with little or no overlap with the learned representations. Both processes coexist at the level of a single synapse, while the invariance is a network-level property.

We investigate this concept by first considering a perfect segregation, i.e., the dynamics of learning and spontaneous fluctuations are completely separable, and do not interfere with one another. We show that the learned representations give rise to stable trajectories of network activity; these memory states can be viewed as the time-varying analogs of stable fixed points in the classical Hopfield model [19]. At later times, the embedded memory items may be retrieved by supplying an associative recall cue. These results show that memory can be learned and retained in a stable manner despite significant ongoing synaptic fluctuations.

Relaxing the assumption of perfect separation leads to an overlap between the dynamics of spontaneous fluctuations and of learning. In this case, memory traces do not

persist indefinitely, but rather their strength decays over time. The extent of overlap between the two contributions to synaptic plasticity, as well as subsequent external stimulation, determine the lifetime of an embedded memory trace.

Finally, our model generates an experimentally testable prediction: when examining pairs of reciprocally connected neurons, the strength of these two synapses is expected to vary both at rest and during learning. The correlation between these variations, however, should be differentially affected, with learning leading to decorrelation.

Results

Model description. Our model is based on a standard framework of firing-rate neural networks [20]. The network consists of N recurrently connected neurons, with the synaptic connection strength from unit j to unit i denoted by W_{ij} . Each neuron i transforms its input x_i into firing rate via a saturating nonlinearity $\phi(x_i)$, where x_i evolves as

$$\dot{x}_i = -x_i + \sum_j W_{ij} \phi(x_j) + b_i(t), \quad (1)$$

and $b_i(t)$ is an external input. This framework, while abstract, has proven useful in capturing qualitative aspects of network-level phenomena [21, 22]. Typically, such models assume that connectivity is fixed; when used for studying functionality and learning, dynamics of neural activity and connectivity are assumed to unfold over separate timescales [19, 23] (but see also [24, 25]). In our framework, the connectivity matrix W co-evolves with neural activity x , albeit with distinct timescales (Fig. 1 - illustration).

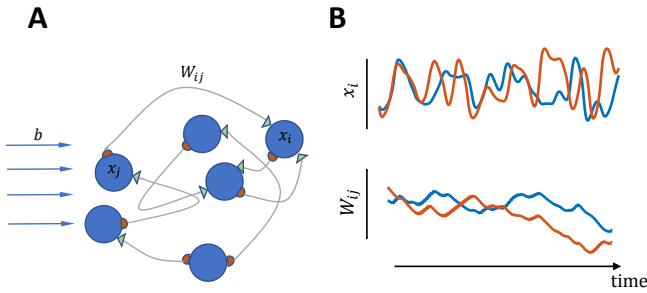


Figure 1: Co-evolution of neural activity and connectivity. (A) Illustration of our modeling framework: a recurrently connected neural network, with W_{ij} denoting the strength of contribution of firing activity of neuron j , $\phi(x_j)$, to a given neuron i . An external signal b_i is assumed as additional input to each neuron i . For the non-linearity we take $\phi(x_i) = \tanh(x_i)$ throughout the text. (B) Both the neural input state (x_i) and each individual connection strength (W_{ij}) evolve over time, though on different timescales, and their dynamics are coupled.

In order to study the coexistence of memory with synaptic fluctuations, we let W evolve due to contributions arising from both learning-related and fluctuation-related terms, denoted by Δ_L and Δ_F respectively:

$$\dot{W} = \Delta_L + \Delta_F. \quad (2)$$

These two terms, describing synaptic plasticity rules, can lead to a decomposition of matrix-space, defining the component of W which would ultimately retain learned information. In principle, almost any decomposition of W , together with appropriate plasticity rules, can allow retention of memory traces alongside spontaneous synaptic fluctuations (see Supplemental Information S1). However, local learning rules observed in experiments (e.g., STDP) have a well-defined directionality: consecutive firing of neuron i before j leads to a strengthening of the connection W_{ji} and to the weakening of the reverse connection. The temporal asymmetry of STDP [18] leads to a strongly asymmetric learning rule when applied to our rate model (Fig. 2A, center). Assuming perfect anti-symmetry, we find the form $\Delta_L \propto \phi y^T - y \phi^T$ (y is a smoothed version of ϕ , see Methods), which in turn modifies only the anti-symmetric component of W (Fig. 2B). The synaptic representation of a given memory is thus encoded by the deviation from symmetry of the connections between pairs of neurons (as suggested by Ref. [25]).

In addition to Hebbian modifications, synaptic connection strengths in our model are assumed to spontaneously drift, each with a different rate. If unrestrained, such dynamics would eventually lead to divergence of W , and preventing divergence may be achieved by activity-dependent homeostatic plasticity. In contrast to the directed nature of STDP, homeostasis is generally expected to be homogeneous in time and across reciprocal connections (Fig. 2A, right; [26]). To establish the concept of a memory-storing component, we first assume perfectly segregated contributions to synaptic plasticity, i.e. the dynamics of learning and fluctuations each evolve separately, and do not mix. Thus, our choice of an anti-symmetric Δ_L implies a purely symmetric fluctuation term Δ_F , and this separation, in turn, entails an orthogonal decomposition of connectivity itself into symmetric (S) and anti-symmetric (A) matrices, $W = A + S$ (Fig. 2B). Relaxing the assumption of perfect segregation will be discussed below.

A specific example of a symmetric term that gives rise to bounded fluctuations is inspired by Ref. [25] and reads $\Delta_F \propto \Sigma - \phi \phi^T$, where Σ is some constant symmetric matrix, and the anti-Hebbian term $-\phi \phi^T$ ensures homeostasis [27]. The interplay between the flux of spontaneous synaptic remodeling and the restraining term gives rise to persistent chaotic dynamics of the symmetric component of W [25] (Fig. 2B, right; see video in S2).

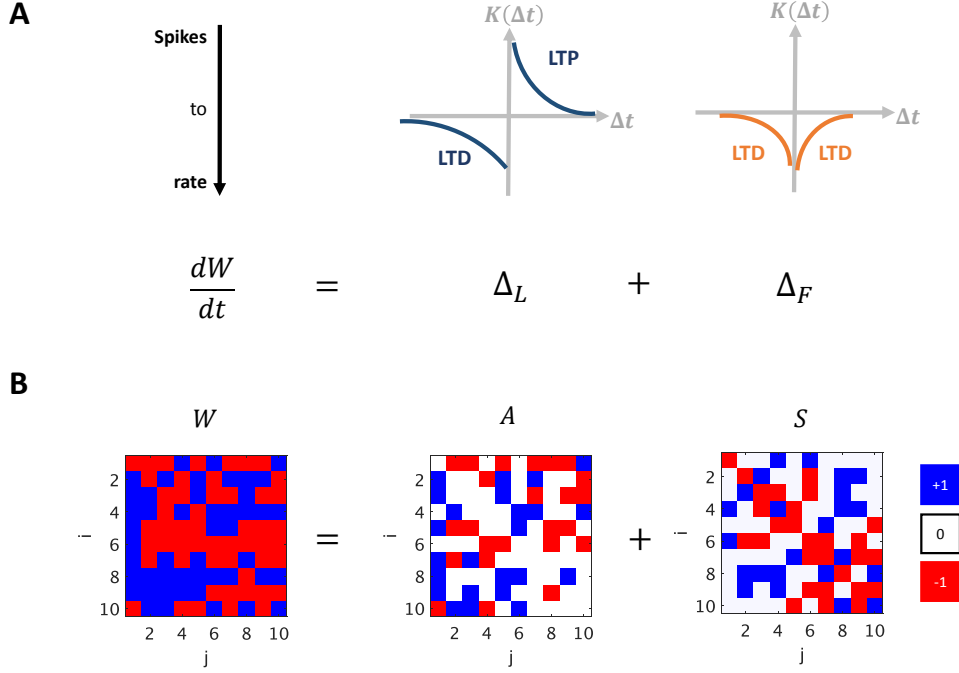


Figure 2: Decomposition of matrix-space. (A) Contributions to synaptic plasticity: from spikes to rates. Top: change in synaptic weight $K(\Delta t)$ as a function of temporal difference in spike timing of the pre- and post-synaptic neurons (see Methods). For STDP, synaptic potentiation and depression are highly asymmetric, but need not be precisely anti-symmetric (left). As a restraining mechanism, we take an anti-Hebbian plasticity term which is symmetric, or very close to such (right). When transitioning from spike-based to rate-based learning, the kernel functions give rise to a highly asymmetric learning rule Δ_L , and a symmetric fluctuation term Δ_F (bottom; see Methods). (B) The contributions to \dot{W} define a decomposition of W itself. Here we illustrate how a random binary 10×10 matrix W is decomposed into a sum of an anti-symmetric matrix A and a symmetric matrix S , which evolve according to Δ_L and Δ_F , respectively.

Overall, combining equations (1) and (2), our model takes the form

$$\begin{aligned} \dot{x} &= -x + W\phi + b, \\ \dot{W} &= \eta_L (\phi y^T - y \phi^T) + \eta_F (\Sigma - \phi \phi^T), \end{aligned} \quad (3)$$

with $\eta_L, \eta_F > 0$ the rates of the respective plasticity terms.

Life-cycle of a memory trace. Our model is capable of forming lasting memory representations of past stimuli and embedding them within the anti-symmetric component of connectivity. Upon presentation of a transient, dynamic input signal $b(t)$ (Fig. 3A, left), the synaptic weights are modified by Δ_L in an activity-dependent manner (see ‘Acquisition’ Section below). Throughout learning and thereafter, Δ_F inflicts irregular modulations to the efficacies of all synapses (Fig. 3B). The extent of asymmetry in Δ_F determines the lifetime of learned memory traces: a purely symmetric fluctuation term corresponds to perfect retention; any overlap with the anti-symmetric component will drive a constant-rate degradation of the internal representations (see ‘Retention’ Section below). Finally, following

learning, the stored patterns can be auto-associatively retrieved, by presenting an appropriate cue. In addition to bounding spontaneous, undirected, synaptic fluctuations, the restraining force also restores homeostasis to neural activity following each retrieval event (Fig. 3A, right; ‘Retrieval’ Section below). We now analyze model behavior throughout the different phases in the lifetime of a memory item.

Acquisition. The acquisition, i.e. the encoding and storage of a new memory trace, is initiated by stimulating the network with an external signal, $b(t)$. Because our learning rule is anti-symmetric, b must effectively span at least two directions for inducing a change to the anti-symmetric component of W . We therefore present the network with an arbitrary time-varying input evolving on a plane spanned by two arbitrary directions $u, v \in \mathbb{R}^N$ (see Methods). As the input drives neural activity x onto the plane spanned by u and v , the activity-dependent learning operator Δ_L follows and becomes non-negligible, which in turn causes a change in the anti-symmetric connectivity component, A .

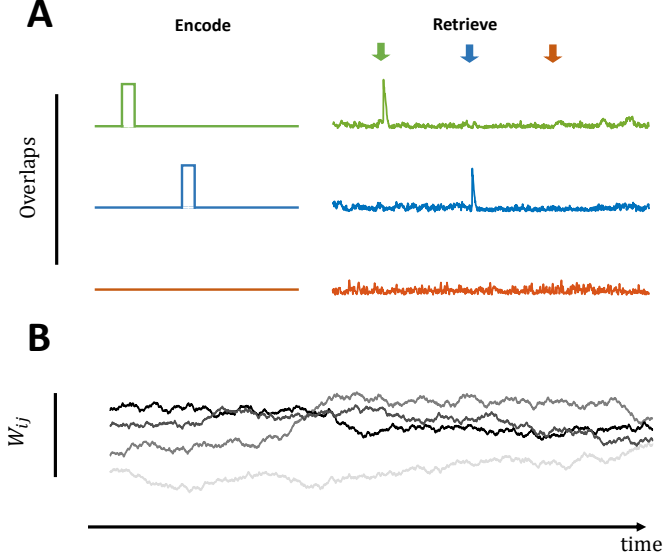


Figure 3: Stable memory with unstable synapses. (A) Left: Schematic of the training protocol. Two distinct stimuli are sequentially presented to the network (green, blue). The learning rule modifies the synaptic matrix as to encode and embed each of the stimuli. Right: Overlaps of the neural state x with the two learned patterns (top and middle trajectories). The learned memories are retained and can be retrieved via appropriate cues: the embedded memories can be read out of the network dynamics via a brief stimulation bearing partial information of the original stimulus (arrows). A novel cue, on the other hand, does not elicit a significant response in neural activity (bottom trajectory, orange). (B) Weights of four out of N^2 synapses (gray shade) as a function of time. The spontaneous and homeostatic contributions to plasticity drive perpetual fluctuations of synaptic weights, which occur during and after learning. Plotted activity and connectivity trajectories are obtained from a simulation of our model with $N = 128$ neurons (see Methods for simulation details).

The learning procedure embeds geometric information of the external stimulus, specifically the directions u and v , within the anti-symmetric part of the connectivity matrix. In particular, the encoding is manifested as a rank-2 matrix $uv^T - vu^T$ which is imprinted into A . To see this, we examine the eigen-decomposition of W . During stimulus presentation, a complex conjugate eigenvalue pair forms (Fig. 4A), and the eigenplane corresponding to this pair overlaps completely with the plane spanned by u, v (Fig. 4B). The strength of the memory representation - corresponding to the magnitude along the imaginary axis of the encoding eigenmode - is a function of stimulation duration and of input amplitude.

Lastly, the learning matrix Δ_L need not be purely anti-symmetric in order to form new memory representations. However, any overlap between Δ_L and the symmetric subspace would be washed away by the spontaneous fluctua-

tions, thus leading to sub-optimal learning (see S3).

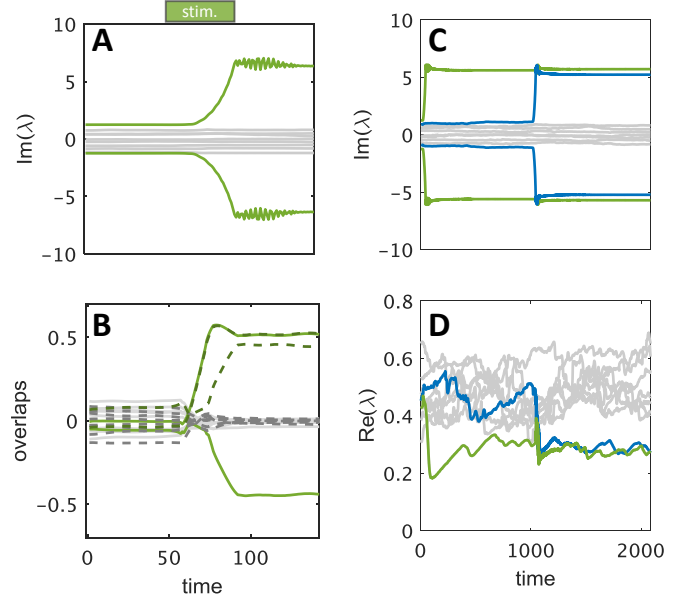


Figure 4: Hebbian learning by STDP embeds persistent anti-symmetric memory representations. Eigen-decomposition of the Jacobian of \dot{x} around the origin, $J = W - I$, as a function of time, before, during and after external stimulation (applied between times $t = 50$ and $t = 100$). (A) Imaginary part of the spectrum $\lambda(J)$ of J over time (shown are 10 out of $N = 128$ eigenvalues). Before learning, the imaginary part of $\lambda(J)$ is almost constant in time. The embedding of a memory item manifests as the growth in imaginary amplitude of one complex conjugate eigenvalue pair (green). (B) During stimulus presentation, the learning rule modifies W such that $u \pm iv$ become eigenvectors. Plotted are the overlaps of the eigenvector of J , corresponding to the largest imaginary eigenvalue (green in A), with N directions: u, v (green), and $N - 2$ orthogonal directions (gray). Real and imaginary parts are shown in full and dashed lines (and, for clarity, light and dark shades), respectively. (C) Zoom-out of panel A. After the stimulus is removed, the memory representation persists (green). A second stimulus, confined to an orthogonal plane, is similarly learned at a later time (blue); both memory items are retained. (D) Real part of $\lambda(J)$ over time. Each memory item is suppressed following learning (green, blue).

Retention of a learned memory item is achieved by means of a dedicated component of network connectivity. With a symmetric fluctuation term as in equation (3), the imaginary part of the spectrum remains unchanged in the absence of external stimuli (Fig. 4A; [25]). This is true also after learning, when a memory item is stored in the network (Fig. 4C, green). Furthermore, subsequent learning episodes can store additional memory items (Fig. 4C, blue). The existence of an embedded memory attracts neural activity to the plane corresponding to the memory item; in turn the anti-Hebbian dynamics in Δ_F induce suppression

of this direction (Fig. 4D, green and blue). In this way, the attractor is implicitly represented by network connectivity, without neural activity bearing any signature of the learned memory. If no other learning events occur, this memory trace will be stored in the network indefinitely (infinite lifetime), while each synaptic weight fluctuates symmetrically.

One may relax the assumption of strictly symmetric fluctuations and still arrive at a functional memory system. In this case, all qualitative features discussed above still hold, but memory traces now have a finite lifetime. To illustrate this, we simulate a network with the fluctuation term

$$\Delta_F \propto \Sigma - f(x)g(x)^T,$$

where Σ is some asymmetric matrix and $f \neq g$ are sigmoidal functions applied element-wise to x . In this case, the anti-symmetric component of W also drifts spontaneously, due to the asymmetry in Σ (we quantify asymmetry by the angle of the matrix from the symmetric subspace, see illustration in Fig. 5A). In order to maintain stable dynamics, these changes must be restrained by the asymmetric component of the activity-dependent homeostatic term fg^T (Fig. 5B, blue). If the asymmetry of Σ is large relative to that of fg^T , homeostasis is not achieved, and the anti-symmetric part of W diverges (Fig. 5B, orange).

In addition to driving asymmetric synaptic fluctuations, the overlap of Δ_F with the anti-symmetric subspace also affects embedded memory traces: the strength of the representation is gradually attenuated, until the memory is completely forgotten. This process is reflected in the decay of the imaginary part of the encoding eigenvalue pair (Fig. 5C); interestingly the decay is approximately linear in time (until it is near the bulk of the spectrum), with a slope that varies across network realizations. The average of this slope depends on the extent of asymmetry of the homeostatic term (Fig. 5D). Thus, in our model there is a tradeoff between memory lifetime, and stability in the face of spontaneous asymmetric fluctuations.

Retrieval. We have seen that biologically-inspired learning rules can capture the orientation of an incoming stimulus in neuronal state-space and encode this information within network connectivity. However, in order for these representations to implement memory items, their information should be retrievable from the network dynamics; a memory item is said to be retrieved if the neural state exhibits an activity pattern resembling the original stimulus. Indeed, we find that learning creates attractors in neural-activity space, similar in fashion to the Hopfield model [19]. To see this most clearly, consider a single memory already embedded in the network by a learning process such as equation

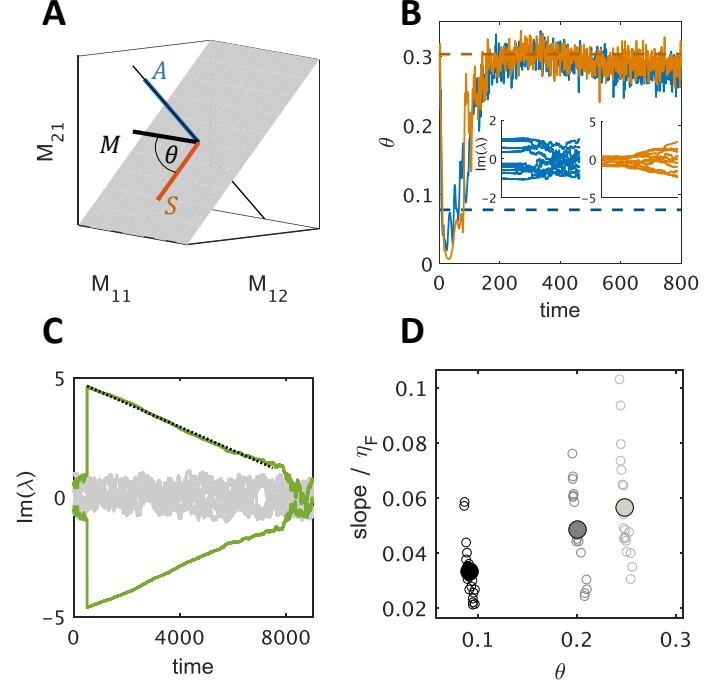


Figure 5: Asymmetric fluctuations and memory degradation. (A) Matrices viewed as vectors in \mathbb{R}^{N^2} , a space which can be decomposed into two orthogonal subspaces: symmetric matrices (gray plane) and anti-symmetric matrices (perpendicular line). The extent of its asymmetry is quantified as the angle θ between the matrix and its projection onto the symmetric subspace, S . (B) The extent of asymmetry of the two terms comprising Δ_F (Σ dashed, fg^T solid) for Σ with low (blue) or high (orange) asymmetry. The restraining term, $f = \tanh(x_i)$ and $g = \tanh(10 \cdot x_i)$, is the same for both cases. The insets show the imaginary part of the spectrum $\lambda(J)$ over time, demonstrating divergence when the restraining term is too close to symmetric. (C) Magnitude of the imaginary part of $\lambda(J)$ over time. A memory plane is stored (by means of equation (3)) within network connectivity at time $t = 500$ (green trajectory), and its strength thereafter degrades linearly with time (dotted black line shows best fit), until it returns to the bulk of $\lambda(J)$. (D) Fitted linear rate of memory decay, plotted against the mean steady-state angle of the restraining force fg^T for many simulations (circles). Various functions g were tested (\tanh with steepness 2, 5 and 10 shown in black, gray and light gray, respectively). The data exhibit a wide spread, but on average a clear dependence is seen (filled circles).

(3), and, for simplicity, we will initially keep W fixed during retrieval. Following the Hopfield paradigm, we write W as:

$$W(t) \equiv W = \rho(uv^T - vu^T), \quad (4)$$

where the coefficient $\rho > 0$ represents the strength of the memory representation [28].

With one stored memory as in equation (4), we find that, from any non-zero initial condition, the dynamics converge to periodic motion concentrated on the memory plane spanned by u and v (Fig. 6A). In the limit of an infinitely

steep nonlinearity ϕ (i.e. a step-function), the full dynamics are well approximated by their projected coordinates on the plane, p_u and p_v ; the low-dimensional system reads

$$\begin{aligned}\dot{p}_u &= -p_u + \rho \arctan\left(\frac{p_v}{|p_u|}\right) \\ \dot{p}_v &= -p_v - \rho \arctan\left(\frac{p_u}{|p_v|}\right),\end{aligned}\quad (5)$$

and, for sufficiently large ρ , exhibits a stable limit-cycle around the origin (see S4). Thus, memory items correspond to dynamic attractors, with geometry defined by that of the stimulating input. During retrieval of the stored memory, neural activity evolves over time, following a well-defined trajectory in state-space. This behavior stands in contrast to the classical symmetric Hopfield model, where memories are represented by fixed-point attractors. Compared to point attractors, time-dependent states better account for retrieval dynamics in neural networks, as suggested by several experimental studies [29, 30].

Embedding multiple memory planes $\{u^{(k)}, v^{(k)}\}_{i=1}^M$ corresponds to setting

$$W = \sum_{k=1}^M \rho_k \left(u^{(k)} v^{(k)T} - v^{(k)} u^{(k)T} \right)$$

Now, a locally stable limit-cycle lies on each embedded plane, and the network functions as an auto-associative memory: initiating the dynamics within the basin of attraction of one plane - providing the network with partial information of the memory to be retrieved - leads to the recovery of the full memory item (Fig. 6B). Numerically, the capacity is comparable with that of the symmetric Hopfield model, however, stable heterogeneous mixtures exist for any memory load $\alpha = M/N \leq 1/2$ (Fig. 6B, [31]; see S5).

Finally, we consider the case of retrieval in the presence of synaptic fluctuations, equation (3). A retrieval event is initiated by inputting a short, high amplitude stimulus to the network, one that has high overlap with the memory item requested for recall. Once stimulation is applied, neural activity converges to the corresponding embedded memory plane (Fig. 6C). During retrieval, the mere presence of the neural state on the attractor causes, through anti-Hebbian plasticity, the real part of the corresponding eigenvalue to decrease (Fig. 6C,D). The visited attractor is then destabilized by the growing suppression, and network activity returns to unstructured, undirected, fluctuations (Fig. 6C; see also Fig. 3B lower trace, which shows that the projection onto the destabilized memory is of similar magnitude to a projection onto a random direction). A refractory period ensues as the suppressing force relaxes back

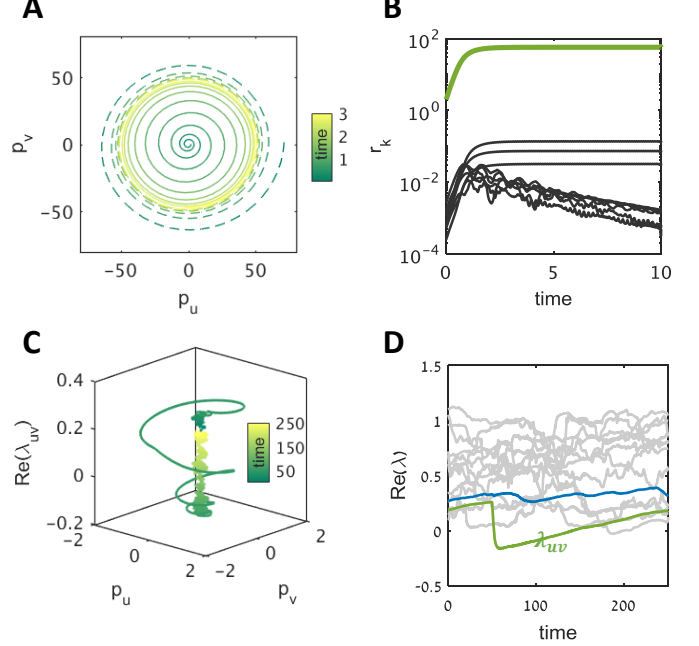


Figure 6: Dynamics of memory retrieval with fixed (top) and fluctuating (bottom) connectivity. (A) Overlaps of network activity x with the two directions spanning one embedded memory plane, $p_u := 1/N u^T x$ and $p_v := 1/N v^T x$, over time (color). Solid and dashed lines represent trajectories initiated inside and outside the stable orbit, respectively. (B) Radial coordinates of overlaps with each of multiple ($M = 10, N = 1024$) embedded memory planes, $r_k := \sqrt{p_{u^{(k)}}^2 + p_{v^{(k)}}^2}$. Initiating the network near one plane, $u^{(1)}, v^{(1)}$, results in convergence to the associated attractor (green). Three of the remaining nine planes have a non-vanishing radius of overlap; this radius, however, is two orders of magnitude smaller than that of the target plane. (C) Real part of the pair of memory-encoding eigenvalues, as a function of p_u, p_v . At time $t = 50$ a stimulus is applied for a duration of 1 time constant. As a result, network activity converges onto the corresponding attractor. As the attractor is destabilized, the activity state slips off the memory plane, and exhibits suppressed, low-amplitude fluctuations on this cross-section. (D) Real part of the spectrum $\lambda(J)$ over time. The green trajectory shows the real part of the eigenvalue pair corresponding to the embedded memory plane; as retrieval is triggered, the real part drops sharply below the equilibrium value. Following is a linear relaxation of suppression, with slope given by η_F . All other eigenvalues, including the ones corresponding to other memory representations (blue), are not affected by retrieval of the memory item.

to equilibrium values, after which the memory item is again fully retrievable (Fig. 6D).

The co-evolution of neural activity and connectivity during retrieval can be understood as a perturbation from equilibrium of a low-dimensional dynamical system (Fig. 6C). In particular, the projections onto the plane p_u, p_v evolve similarly to equation (4), but the stability of the attractor depends on the real part of the eigenvalue associated with the learned memory plane, which is now itself a dynamical variable. We derive and discuss the three-dimensional system in S6.

Discussion

Overall, we showed that it is possible to store and retrieve memories in the face of strong activity-independent synaptic fluctuations. Our approach is motivated by a combination of physiological observations (temporal asymmetry of STDP) and mathematical considerations (symmetry of homeostatic mechanisms), which leads to a natural segregation of synaptic connectivity-space into two components: one stores memories while the second fluctuates chaotically. In this manner, a global combination of synapses remains invariant, while every individual synapse fluctuates. This approach offers a link between learning rules at the single-synapse level, and global memory encoding at the systems level.

Our analysis allows us to extend the classical, symmetric Hopfield model to the case where memories are represented by trajectories in neural state space [28], rather than static activity patterns. This temporal dependence is more consistent with some experimental observations: the oscillatory trajectories of memory-trace activations that arise naturally in our model resemble network-level oscillations observed during memory retrieval [29] and consolidation [30]. The symmetric Hopfield network is highly stable against static synaptic noise [32], and this is also true for certain classes of dynamic noise sources. However, the synaptic connectivity matrix would in general diverge (e.g. when assuming a biased external noise), and thus a restraining term is necessary. As discussed above, homeostasis requires the restraining term to significantly overlap with the symmetric matrix subspace. With such connectivity dynamics, the symmetric encodings deteriorate, and retention of embedded memories requires some form of reinforcement, e.g. rehearsal of the stored memories [24, 33]. In our model, noise is internally generated by the interplay between spontaneous fluctuations and homeostatic control; by virtue of the highly asymmetric encoding, memories nevertheless persist. This finding is in-line with recent computational studies, which found that purely anti-symmetric STDP kernels give rise to stable memory traces, whereas deviation

from anti-symmetry entails memory degradation [24, 34]. Our work puts this idea into a more general framing: regardless of the chosen decomposition, optimal learning and retention are achieved only with orthogonal contributions to synaptic dynamics, whereas an overlap leads to decay of the memory trace.

Our choice of the anti-symmetric subspace as invariant generates a prediction which can be assessed directly from neural data: the temporal evolution of effective connectivity weights between a reciprocally connected pair of neurons should be highly correlated in the absence of learning, since our model predicts that in this case fluctuations occur mainly in the symmetric component of connectivity. If sampled during a learning epoch, this correlation should decrease, since in this case the change in connectivity is highly asymmetric (see S7). Given access to a larger sample of a memory engram cell-ensemble [35], one may even compute the overlap between learning-induced modifications and spontaneous fluctuations. With such data, our framework makes predictions which may extend to the behavioral level: larger overlaps lead to faster decay of memory traces (see Fig. 5), or to persistent but weaker memories (see S3).

Methods

Model simulation

We use home-made MATLAB software in order to simulate equation (3). The spectra of matrices are computed using built-in MATLAB functions, and their time-series sorted using the eigenshuffle MATLAB script, freely available online. For the nonlinearity in firing rates, we use the hyperbolic tangent function, $\phi(z) = \tanh(z)$. For all figures we simulate a network with $N = 128$ neurons, except for the anti-symmetric Hopfield model in Fig. 6A,B where we use $N = 1024$. Simulations with larger networks similarly exhibit all of the discussed phenomena. For numerical integration we use a time constant $dt = 10^{-2}$. The learning-rate parameters are taken as $\eta_F = 10^{-3}$ and $\eta_L = 10^{-2}$. For the low-pass filter y , we use a second-order filter with natural frequency $\omega_n = 2\pi$ and damping term $\zeta = 10^{-3}$ (see next Methods section). For the learning process we use the time-dependent input $b(t) = c_u(t)u + c_v(t)v$ with memory patterns $u^{(k)}, v^{(k)} \in \{\pm 1/\sqrt{N}\}^N$ taken to be orthogonal; the time-dependent functions are taken as $c_u(t) = \sqrt{N}\cos\omega_n t$ and $c_v(t) = \sqrt{N}\sin\omega_n t$, or alternatively, $c_u(t)$ and $c_v(t)$ each following an independent constrained Brownian motion.

Derivation of plasticity rules

Our starting point is a Poisson spiking neuron with output spiking activity $S_i(t)$ and instantaneous firing rate $\phi_i(t)$ [36]. STDP learning is characterized by a differential update of the synaptic

efficacy W_{ij} , based on the temporal distance Δt between spiking of unit i and unit j ; the amplitude of change is given by the learning window $K(\Delta t)$ [18] (see Fig. 2). Following [36], we denote the correlation between inbound and outbound spiking activity by

$$C_{ij}(t; t + \Delta t) = \overline{\langle S_i(t) S_j(t + \Delta t) \rangle},$$

where angular brackets denote ensemble averaging over the noise in spiking activity and overbar denotes temporal averaging. Neglecting first-order contributions from spiking activity, we write the weight change as

$$\begin{aligned} \dot{W}_{ij} = & \eta_L \int_{-\infty}^t ds K(t-s) C_{ij}(t; s) \\ & + \eta_L \int_{-\infty}^t ds K(s-t) C_{ij}(s; t) \end{aligned}$$

[24]. To proceed, we approximate the correlation, writing it in terms of the instantaneous firing rates $C_{ij}(t; s) \approx \phi_i(t) \phi_j(s)$ [36], and assume a learning window of the form

$$K(\Delta t) = \begin{cases} a_P e^{-\tau_P \Delta t} & \Delta t > 0 \\ a_D e^{\tau_D \Delta t} & \Delta t \leq 0 \end{cases}$$

where $a_P, \tau_P, \tau_D > 0$ and $a_D < 0$ (Fig. 2). Performing the integration, we obtain

$$[\Delta_L]_{ij} = \eta_L \left(a_P \phi_i(t) y_j^P(t) - \phi_j(t) y_i^D(t) \right).$$

where y^P, y^D are first-order low-pass filters of spiking rates ϕ ; each filter is characterized by a different timescale, τ_P and τ_D respectively.

In general, the parameters of K give rise to an asymmetric learning operator Δ_L . The extent of asymmetry is determined by the discrepancy between the two pairs of kernel parameters, i.e. the difference in timescales of potentiation and depression τ_P, τ_D , and the two amplitudes a^P, a^D . When $\tau_D = \tau_P$ and $a_D = -a_P$, the resulting learning operator is purely anti-symmetric:

$$[\Delta_L]_{ij} = a_P (\phi_i y_j - \phi_j y_i).$$

The anti-symmetric learning operator Δ_L constructed above drives maximal change to connectivity when the vectors y, ϕ are orthogonal. Now, for the first-order filter arising from the choice of K above, a phase response of $-\pi/2$ is achieved only in the limit of an infinite frequency, the regime in which the output amplitude is close to zero. In order to ameliorate the learning procedure, we therefore construct Δ_L by choosing for y a second-order filter defined by

$$\ddot{y} + 2\zeta\omega_n \dot{y} + \omega_n^2 y = \omega_n \phi;$$

now, on the contrary, maximal amplitude response is achieved exactly at the frequency admitting a phase response of $-\pi/2$ ($\approx \omega_n$).

In a similar way we can derive a symmetric rate-based anti-Hebbian learning rule. For this, we use a kernel K with parameters $\tau_D = \tau_P$ and $a_P = a_D < 0$, and, explicitly inserting an activity-independent contribution we arrive at

$$[\Delta_F]_{ij} = \Sigma_{ij} - a_P (\phi_i y_j + \phi_j y_i).$$

For simplicity of analysis, we approximate $[\Delta_F]_{ij} \approx \Sigma_{ij} - \phi_i \phi_j$.

References

- [1] A. Dickinson N. S. Clayton, T. J. Bussey. Can animals recall the past and plan for the future? *Nat. Rev. Neurosci.*, 2003.
- [2] Michael J. Kahana. *Foundations of human memory*. Oxford Press, 2012.
- [3] M. Poo, , M. Pignatelli, and C. Stevens. What is memory? the present state of the engram. *BMC Biol.*, 2016.
- [4] R.Y. Tsien. Very long-term memories may be stored in the pattern of holes in the perineuronal net. *Proc. Natl. Acad. Sci. USA*, 2013.
- [5] N. Brunel H. K. Titley and C. Hansel. Toward a neurocentric view of learning. *Neuron*, 2017.
- [6] G. Bi and M. Poo. Synaptic modification by correlated activity: Hebb's postulate revisited. *Annu Rev Neurosci.*, 2001.
- [7] G. Mongillo, S. Rumpel, and Y. Loewenstein. Intrinsic volatility of synaptic connections a challenge to the synaptic trace theory of memory. *Curr. Opin. Neurobiol.*, 2017.
- [8] C. Clopath, T. Bonhoeffer, M. Hubener, and T. Rose. Variance and invariance of neuronal long-term representations. *Philos Trans R Soc Lond B Biol Sci.*, 2017.
- [9] A. R. Chambers and S. Rumpel. A stable brain from unstable components: Emerging concepts and implications for neural computation. *Neuroscience*, 2017.
- [10] N. Ziv N. Brenner. Synaptic tenacity or lack thereof: Spontaneous remodeling of synapses. *Trends Neurosci.*, 2017.
- [11] A. Minerbi, R. Kahana, L. Goldfeld, M. Kaufman, S. Marom, and N. E. Ziv. Long-term relationships between synaptic tenacity, synaptic remodeling, and network activity. *PLoS Comput Biol*, 2009.
- [12] R. Dvorkin and N. E. Ziv. Relative contributions of specific activity histories and spontaneous processes to size remodeling of glutamatergic synapses. *PLoS Biol.*, 2016.
- [13] N. Yasumatsu, M. Matsuzaki, T. Miyazaki, J. Noguchi, and H. Kasai. Principles of long-term dynamics of dendritic spines. *J Neurosci.*, 2008.
- [14] Y. Loewenstein, U. Yanover, and S. Rumpel. Predicting the dynamics of network connectivity in the neocortex. *The Journal of Neuroscience*, 2015.
- [15] G. Yang Gan, F. Pan, and W.B. Stably maintained dendritic spines are associated with lifelong memories. *Nature*, 2009.

- [16] H. J. Koester and D. Johnston. Target cell-dependent normalization of transmitter release at neocortical synapses. *Science*, 2005.
- [17] T. Fares and A. Stepanyants. Cooperative synapse formation in the neocortex. *Proc. Natl. Acad. Sci. USA*, 2009.
- [18] G. Bi and M. Poo. Synaptic modifications in cultured hippocampal neurons: dependence on spike timing, synaptic strength, and postsynaptic cell type. *J Neurosci*, 1998.
- [19] J. J. Hopfield. Neural networks and physical systems with emergent collective computational abilities. *Proc. Natl Acad. Sci. USA*, 1982.
- [20] P. Dayan and L. F. Abbott. *Theoretical Neuroscience: Computational And Mathematical Modeling of Neural Systems*. MIT Press, 2005.
- [21] V. Mante, D. Sussillo, K. V. Shenoy, and W. T. Newsome. Context-dependent computation by recurrent dynamics in prefrontal cortex. *Nature*, 2003.
- [22] H. Sompolinsky C. van Vreeswijk. Chaos in neuronal networks with balanced excitatory and inhibitory activity. *Science*, 1996.
- [23] O. B. Amaral R. Osan, A. B. L. Tor. A mismatch-based model for memory reconsolidation and extinction in attractor networks. *PLoS One*, 2011.
- [24] Y. Wei and A. A. Koulakov. Long-term memory stabilized by noise-induced rehearsal. *J. Neurosci.*, 2014.
- [25] M. O. Magnasco, O. Piro, and G. A. Cecchi. Self-tuned critical anti-hebbian networks. *Phys. Rev. Lett.*, 2009.
- [26] B. Doiron A. Kumar. Formation and maintenance of neuronal assemblies through synaptic plasticity. *Nature Communications*, 2014.
- [27] Michael Holicki Michael Herrmann and Ralf Der. On ashby’s homeostat: A formal model of adaptive regulation.
- [28] A.C.C. Coolen. *Theory of Neural Information Processing Systems*. Oxford University Press, 2005.
- [29] C. A. Skarda and W. J. Freeman. How brains make chaos in order to make sense of the world. *Behav Brain Sci*, 1987.
- [30] D. Par, D. R. Collins, and J. G. Pelletier. Amygdala oscillations and the consolidation of emotional memories. *Trends in Cognitive Sciences*, 2002.
- [31] D. J. Amit, H. Gutfreund, and H. Sompolinsky. Storing infinite numbers of patterns in a spin-glass model of neural networks. *Phys. Rev. Lett.*, 1985.
- [32] H. Sompolinsky. Neural networks with nonlinear synapses and a static noise. *Phys. Rev. A*, 1986.
- [33] G. M. Wittenberg, M. R. Sullivan, and J. Z. Tsien. Synaptic reentry reinforcement based network model for long-term memory consolidation. *Hippocampus*, 2002.
- [34] Y. Park, W. Choi, and S.B. Paik. Symmetry of learning rate in synaptic plasticity modulates formation of flexible and stable memories. *Scientific Reports*, 2017.
- [35] P. T. Pang C. B. Puryear A. Govindarajan K. Deisseroth S. Tonegawa X. Liu, S. Ramirez. Optogenetic stimulation of a hippocampal engram activates fear memory recall. *Nature*, 2012.
- [36] R. Kempter, W. Gerstner, and J. L. van Hemmen. Hebbian learning and spiking neurons. *Physical Review E*, 1999.
- [37] J. J. Hopfield. Neurons with graded response have collective computational properties like those of two-state neurons. *Proc. Natl. Acad. Sci. USA*, 1984.
- [38] E. Goles. Antisymmetrical neural networks. *Discrete Appl. Math.*, 1986.
- [39] I. Kanter and H. Sompolinsky. Associative recall of memory without errors. *Phys. Rev. A*, 1987.
- [40] F. Mastrogiuseppe and S. Ostojic. Linking connectivity, dynamics, and computations in low-rank recurrent neural networks. *Neuron*, 2018.

Supplementary information

S1 Arbitrary decomposition of matrix space

A central notion in our framework is that of a specific connectivity component mediating memory storage; that is to say, an invariant subspace of $\mathbb{R}^{N \times N}$ within which information is encoded. Motivated by biological observations, in the main text we focused on a particular such subspace, that comprised of the anti-symmetric matrices. Here, we demonstrate the generality of our framework, by showing that $\mathbb{R}^{N \times N}$ can be decomposed arbitrarily, with one component fluctuating chaotically while the other is invariant. To do so, we simulate a network with neural dynamics following Eq. (1) in the main text. Throughout our analysis, we use the fact that $\mathbb{R}^{N \times N} \simeq \mathbb{R}^{N^2 \times 1}$, i.e. the space of $N \times N$ matrices is isomorphic to the space of vectors of length N^2 , the "vectorizations" of the respective matrices.

For the connectivity dynamics, we project the fluctuation term

$$\Delta_F = \Sigma - f(x)g(x)^T$$

(with $f(x) = \tanh(x)$ and $g(x) = \tanh(10 \cdot x)$) onto a random subspace of \mathbb{R}^{N^2} of arbitrary dimension $M < N^2$. Technically, we construct the orthogonal projection operator

$$P = \sum_{i=1}^M b_i b_i^T,$$

with $\{b_i\}_{i=1}^M \subset \mathbb{R}^{N^2}$ an orthonormal basis; note that P is a linear operator on \mathbb{R}^{N^2} , and as such it is a matrix in $\mathbb{R}^{N^2 \times N^2}$. The dynamics of W then read

$$\dot{W} = \eta_F P \Delta_F,$$

where W , Δ_F denote vectorizations of the corresponding matrices. As a result, we get ongoing bounded fluctuations of the P -component of connectivity (Fig. S1A), and, by definition, the $D = N^2 - M$ dimensional orthogonal complement is invariant (Fig. S1B). Clearly, each individual synapse exhibits ongoing fluctuations (not shown).

One could hypothesize learning rules that operate on the Q -component of connectivity ($Q = I - P$ with I the identity matrix on \mathbb{R}^{N^2}), but we do not present such an example here. Since the P - Q decomposition does not in general align with the symmetric and anti-symmetric subspaces, both real and imaginary parts of the spectrum now fluctuate significantly (Fig. S1C).

S2 Eigenvalues video

==Link==

S3 Relaxing the assumption of purely anti-symmetric learning

Here we show that, under the assumption of symmetric homeostatic fluctuations, learning with rules that are generally asymmetric is possible, but is inferior to the case of pure anti-symmetric rules. We denote the symmetric and anti-symmetric matrix subspaces by \mathcal{S} and \mathcal{A} , respectively, and assume a symmetric fluctuation term, that is, $\Delta_F \in \mathcal{S}$.

First, for a purely anti-symmetric learning operator, i.e. $\Delta_L \in \mathcal{A}$, the overlap in matrix-space between contributions to connectivity dynamics is

$$\Delta_F \cdot \Delta_L = 0,$$

with \cdot denoting the Frobenius inner product. This is true since \mathcal{A} and \mathcal{S} are orthogonal subspaces of \mathbb{R}^{N^2} .

More generally, an asymmetric learning rule can be written in terms of its symmetric and anti-symmetric components, $\Delta_L = \Delta_L^{\mathcal{S}} + \Delta_L^{\mathcal{A}}$, and now

$$\Delta_F \cdot \Delta_L = \Delta_F \cdot \Delta_L^{\mathcal{S}} \neq 0.$$

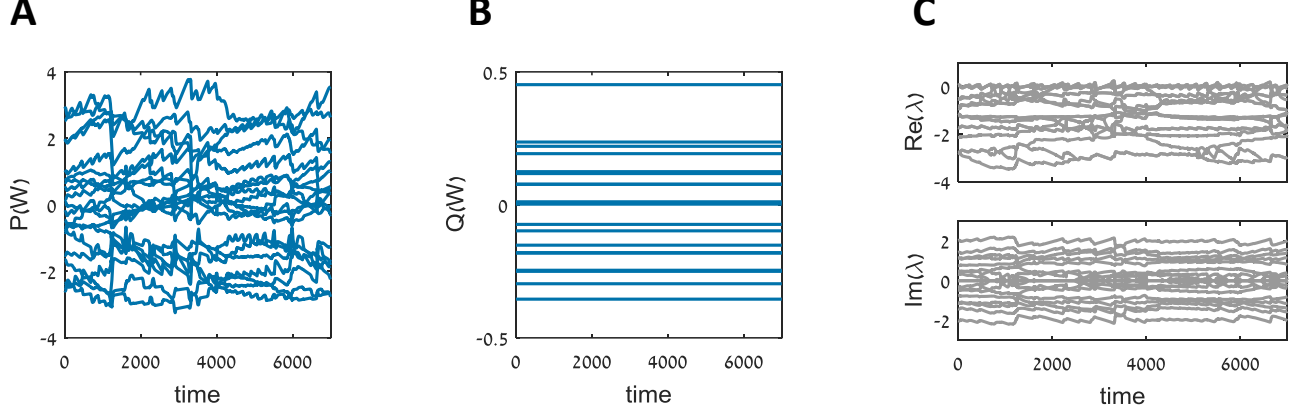


Figure S 1: Arbitrary invariant connectivity subspace. (A) Coordinates of the connectivity matrix W in the P -basis, as a function of time. Here we simulate $N = 20$ neurons, and the fluctuating subspace is of dimension $M = 20$. (B) Coordinates of the connectivity matrix W in the Q -basis, as a function of time. The invariant subspace is of dimension $D = N^2 - M = 380$, and for clarity we present here only 20 coordinates. (C) Real (top) and imaginary (bottom) parts of the eigenvalues of W , as a function of time. As opposed to the symmetric/anti-symmetric decomposition, the imaginary part of the spectrum now also fluctuates.

Any stimulus-related information that propagates to this nonzero overlap will effectively be washed away by the homeostatic force induced by Δ_F , and will not contribute to the learned memory representation. Thus, due to orthogonality, and since $\|\Delta_L^S\| > 0$, we have

$$\|\Delta_L^A\| = \|\Delta_L\| - \|\Delta_L^S\| \leq \|\Delta_L\|,$$

i.e., an optimal norm is achieved only by a purely anti-symmetric learning rule.

We demonstrate the effects of learning with generally asymmetric matrices by constructing a learning rule from non-identical filters y^P, y^D (see Methods). Specifically, we fix the parameters of y^P , and vary the natural frequency of y^D . As the discrepancy between the two filters grows, so does the strength of the resulting memory representation (Fig. S3A). The reduction in learning efficiency strongly depends on the extent of asymmetry of the learning rule Δ_L , as can be seen in the correlation in Fig. S3B.

Note that with this parameterization of asymmetry, any deviation from pure anti-symmetry results in an abrupt drop in the memory representation strength achievable by Δ_L .

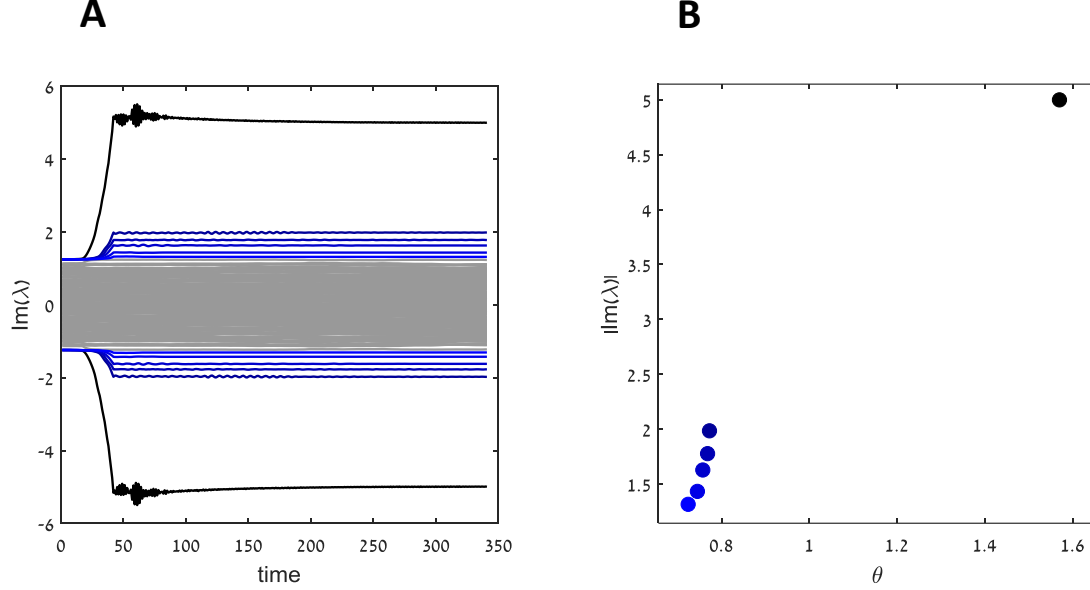


Figure S 3: Overlap with symmetric component degrades learning. (A) Imaginary part of the spectrum of W as a function of time, during learning. We simulate a network with $N = 128$ neurons, and apply an input at times $0 \leq t \leq 40$. As in the main text, we construct learning operators using second order low-pass filters y of neural firing rate ϕ , defined by $\ddot{y} + 2\zeta\omega_n\dot{y} + \omega_n^2 y = \omega_n \phi$. For y^P we take $\omega_n = 2\pi$ and $\zeta = 10^{-3}$. Optimal learning is achieved with a purely anti-symmetric learning rule (black; $y^D = y^P$). The further Δ_L is from anti-symmetry, the lower the resulting memory representation strength (shades of blue; for y^D we take $\omega_n = 2\pi \cdot (\frac{3}{2})^i$ for iteration $1 \leq i \leq 5$). (B) Final amplitude of imaginary part of encoding eigenvalues, as a function of the angle θ between Δ_L and \mathcal{S} . A positive correlation is clearly seen.

S4 Retrieval dynamics: a low-dimensional approximation

In the main text, neural dynamics during retrieval of an embedded memory were shown to converge to a limit-cycle attractor. Here we show that these dynamics can be well approximated by a two-dimensional system.

Consider the neural dynamics presented in Eq. (1) in the main text:

$$\dot{x} = -x + W\phi(x), \quad (1)$$

where one memory plane is embedded into the fixed connectivity:

$$W = \rho(uv^T - uv^T),$$

for $u, v \in \mathbb{R}^N$ with independently drawn, Normally distributed components; the vectors are scaled to have unit norm. Define the macroscopic parameters

$$p_u := u^T x / \sqrt{N}, \quad p_v := v^T x / \sqrt{N},$$

so, from Eq. (1) we have

$$\begin{aligned} \dot{p}_u &= -p_u + \rho v^T \phi / \sqrt{N} \\ \dot{p}_v &= -p_v - \rho u^T \phi / \sqrt{N}. \end{aligned} \quad (2)$$

For large ρ , the overlaps p_u, p_v are also large, so, assuming x is on the plane (all other directions are stable), $x = p_u u + p_v v$, and we approximate the sigmoid ϕ by a step-function:

$$\phi_i(x_i) = \text{sign}[p_u u_i + p_v v_i].$$

Thus, we can approximate the second summand in Eq. (2) by

$$\begin{aligned}
q_v &:= v^T \phi / \sqrt{N} \approx \sum_i v_i \text{sign} [p_u u_i + p_v v_i] / \sqrt{N} \\
&= \sum_i |v_i| \text{sign} \left[p_u \frac{u_i}{v_i} + p_v \right] / \sqrt{N} \\
&= \frac{1}{\sqrt{N}} \sum_i |v_i| s_i;
\end{aligned} \tag{3}$$

for convenience, we have defined $s_i := \text{sign} \left[p_u \frac{u_i}{v_i} + p_v \right]$. Using this representation, we wish to express the macroscopic variables q_u , q_v as functions of p_u , p_v . First, by definition

$$s_i = 1 \iff p_v > -\frac{u_i}{v_i} p_u.$$

Second, since u_i , v_i are independent Normal random variables, the quotient $a := -\frac{u_i}{v_i}$ has a standard Cauchy distribution, with cumulative distribution function

$$\Pr(a \leq x) = \frac{1}{\pi} \arctan(x) + 1/2.$$

Thus,

$$\Pr(s_i = 1) = \Pr(ap_u < p_v).$$

Assume first that $p_u > 0$, so

$$\begin{aligned}
\Pr(ap_u < p_v) &= \\
\Pr\left(a < \frac{p_v}{p_u}\right) &= \frac{1}{\pi} \arctan\left(\frac{p_v}{p_u}\right) + 1/2.
\end{aligned}$$

For $p_u < 0$ we have

$$\begin{aligned}
\Pr(ap_u < p_v) &= \\
\Pr\left(\frac{p_v}{p_u} < a\right) &= 1 - \Pr\left(\frac{p_v}{p_u} > a\right) = -\frac{1}{\pi} \arctan\left(\frac{p_v}{p_u}\right) + 1/2.
\end{aligned}$$

In total, we get

$$\Pr(s_i = 1) = \frac{\text{sign}[p_u]}{\pi} \arctan\left(\frac{p_v}{p_u}\right) + 1/2.$$

For $s_i = -1$ we similarly obtain

$$\Pr(s_i = -1) = \Pr\left(\frac{p_v}{p_u} < a\right) = -\frac{\text{sign}[p_u]}{\pi} \arctan\left(\frac{p_v}{p_u}\right) + 1/2.$$

The expected value for s_i is then

$$\begin{aligned}
\langle s \rangle_{u,v} &= (+1) \Pr(s_i = 1) + (-1) \Pr(s_i = -1) \\
&= \frac{2}{\pi} \text{sign}[p_u] \arctan\left(\frac{p_v}{p_u}\right).
\end{aligned}$$

Inserting this into the sum in Eq. (3), approximating $|v_i| \approx \sqrt{\frac{2}{N\pi}}$ (the expectation of the absolute value of a Normally distributed variable), and neglecting the correlations between $|v_i|$ and s_i , we obtain

$$q_v = \frac{1}{\sqrt{N}} \sum_i |v_i| s_i \approx \left(\frac{2}{\pi}\right)^{3/2} \text{sign}[p_u] \arctan\left(\frac{p_v}{p_u}\right),$$

and a similar derivation gives us

$$q_u := u^T \phi / \sqrt{N} \approx \left(\frac{2}{\pi}\right)^{3/2} \text{sign}[p_v] \arctan\left(\frac{p_u}{p_v}\right).$$

Finally, inserting into Eq. (2) and taking the oddity of $\arctan(\cdot)$ into account, we have

$$\begin{aligned} \dot{p}_u &= -p_u + \tilde{\rho} \arctan\left(\frac{p_v}{|p_u|}\right) \\ \dot{p}_v &= -p_v - \tilde{\rho} \arctan\left(\frac{p_u}{|p_v|}\right), \end{aligned} \quad (4)$$

with $\tilde{\rho} := \rho \left(\frac{2}{\pi}\right)^{3/2}$.

Both the full system Eq. (1) and the approximate system Eq. (4) have a locally stable fixed point at the origin. However, through the approximate system we see that if $\tilde{\rho}$ is large with respect to the dynamic range of p_u, p_v , trajectories would be repelled from the origin. Instead, the two-dimensional system converges to clock-wise rotation around the origin. Numerically, this is an isolated, attracting orbit (Fig. S4).

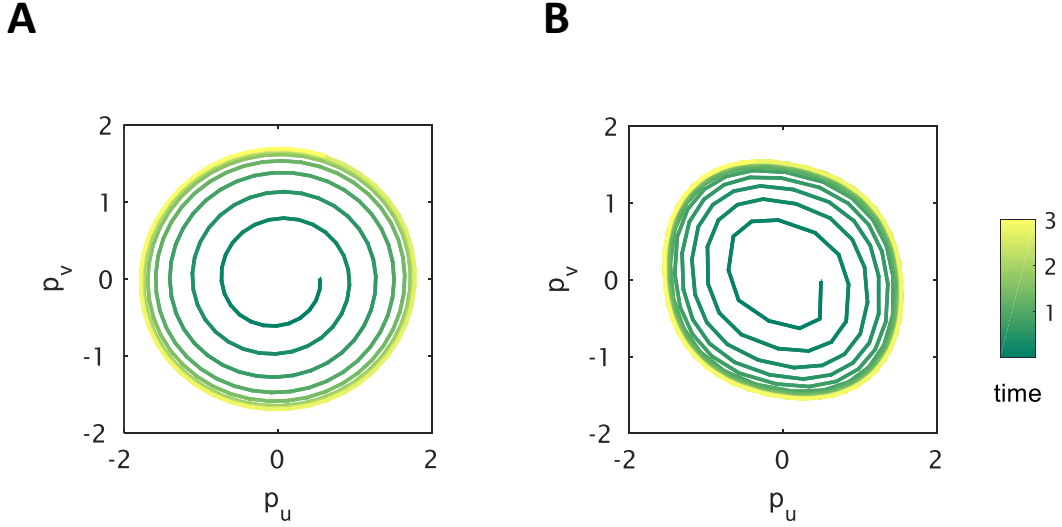


Figure S 4: Dynamics in the full (A) and approximate (B) systems. (A) Projections of neural activity x of the full system Eq. (1), onto the two directions spanning the plane, p_u, p_v (time: color coded). (B) Simulation of the approximate system Eq. (4), which mimics the dynamic behavior of the full system, including the radius of the limit-cycle.

S5 Capacity of the 'Limit-cycle Hopfield' model

In this section we numerically assess the capacity of our anti-symmetric variant of the Hopfield model, and compare it to the classical, symmetric case [19, 37].

We first consider the case of discrete network dynamics [19]:

$$S_i(t+1) = \text{sign} \left[\sum_j W_{ij} S_j(t) \right]. \quad (5)$$

In this setting, and under parallel update dynamics, it has been shown that with purely anti-symmetric connectivity, the dynamics converge to a stable 4-cycle [38]. This result assumes an arbitrary anti-symmetric matrix W ; in our model, as discussed in Section 2.3 of the main text, we consider anti-symmetric matrices formulated as:

$$W = \sum_{k=1}^M \rho_k \left(u^{(k)} v^{(k)T} - v^{(k)} u^{(k)T} \right).$$

The stable cycles arising from this connectivity are precisely $\{\pm u^{(k)}, \pm v^{(k)}\}$, thus linking the result of [38] to the geometry of the eigenspace of W .

In the limit $N, M \rightarrow \infty$, the capacity of the classical Hopfield network constructed of an orthogonal set of memory patterns is $\alpha = \lim_{N, M \rightarrow \infty} M/N = 1/2$ [39]. For $\alpha \leq 1/2$, only the stored memory patterns and their negations are stable fixed-points of the dynamics. However, when $\alpha > 1/2$, the set of fixed-points also includes points which result from flipping individual bits in the original memory patterns. Indeed, the symmetric Hopfield network shows a sharp decrease in recall accuracy for $\alpha > \sim 1/2$ (Fig. S5-1, blue). Interestingly, our anti-symmetric variant exhibits not only perfect accuracy for $\alpha \leq 1/2$, but markedly higher performance compared to the classical Hopfield model when $\alpha > 1/2$.

The qualitatively different decrease of performance may be due to the inherently different properties of the respective matrix classes. Specifically, anti-symmetric matrices by definition have a vanishing diagonal; thus, the dynamics in Eq. (5) are less sensitive to single bit-flips, and it is thus far less probable that spurious cycles would arise. In addition, the stability of a spurious attractor depends now on the conjunction of 4 consecutive and consistent crossover errors, as opposed to one such event in the symmetric Hopfield model.

Next, we compare our model to the continuous version of the classical Hopfield network [37]. For both model variants, the retrieval accuracy is (as expected) slightly lower than the discrete case, especially for larger value of α (Fig. S5-2). Similarly to the discrete case, we find that the anti-symmetric variant performs better than the symmetric one. The transition over $\alpha = 1/2$ is now smooth, and not sharp as in the discrete case.

Finally, we note that once the memory patterns $\{u, v\}$ are not orthogonal, the classical symmetric model outperforms the anti-symmetric model. This is true for both the discrete and continuous cases.

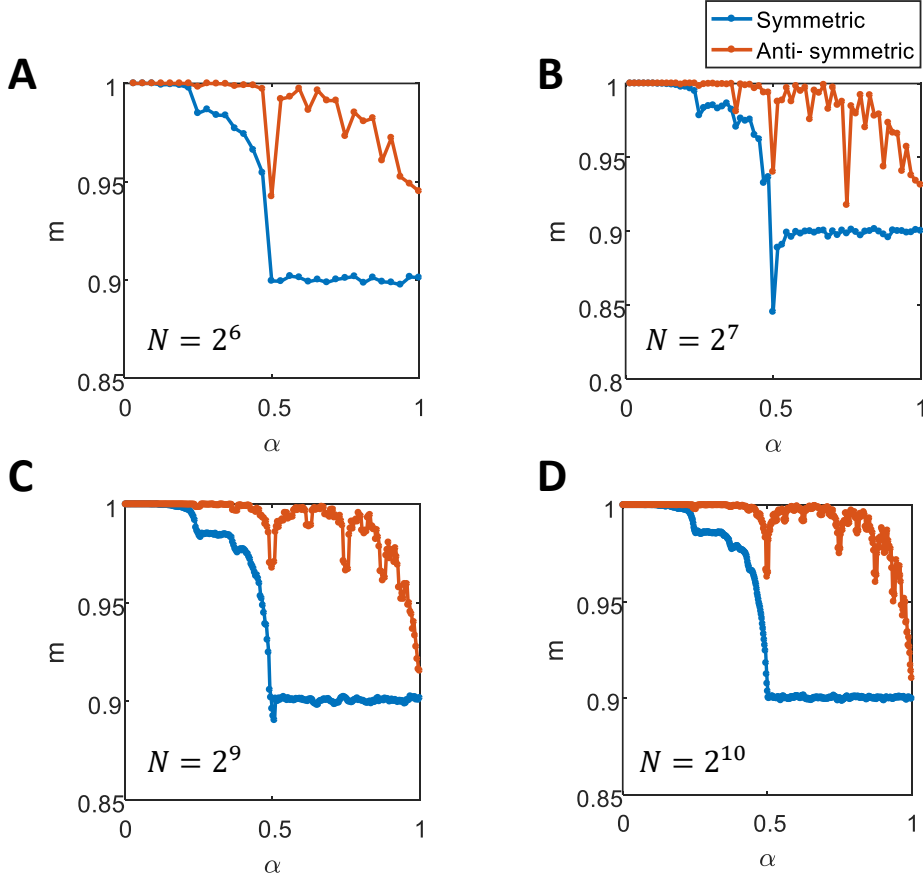


Figure S 5: Capacity of the discrete Hopfield model. Overlap with a target memory item as a function of memory loading $\alpha = M/N$, in the classical Hopfield model (blue) and in our anti-symmetric variant (orange), for various network sizes (A-D; network size N is denoted in each panel). In each instance, the network is initiated at a noisy version of the target pattern, achieved by randomly flipping 5% of the bits in the target. For the classical Hopfield model, the overlap is defined as $m = u^T S / \sqrt{N}$; for the anti-symmetric variant, the overlap is quantified as the L_1 radius on each embedded plane, $m = |q_u| + |q_v|$, with $q_u = u^T S / \sqrt{N}$. For each model, the memory loading M represents the total dimensionality of memory-space: in the symmetric model this corresponds to M distinct memory patterns; in the anti-symmetric variant, this means $M/2$ distinct memory planes. In all cases we use binary $(\pm \frac{1}{\sqrt{N}})$ orthonormal patterns.

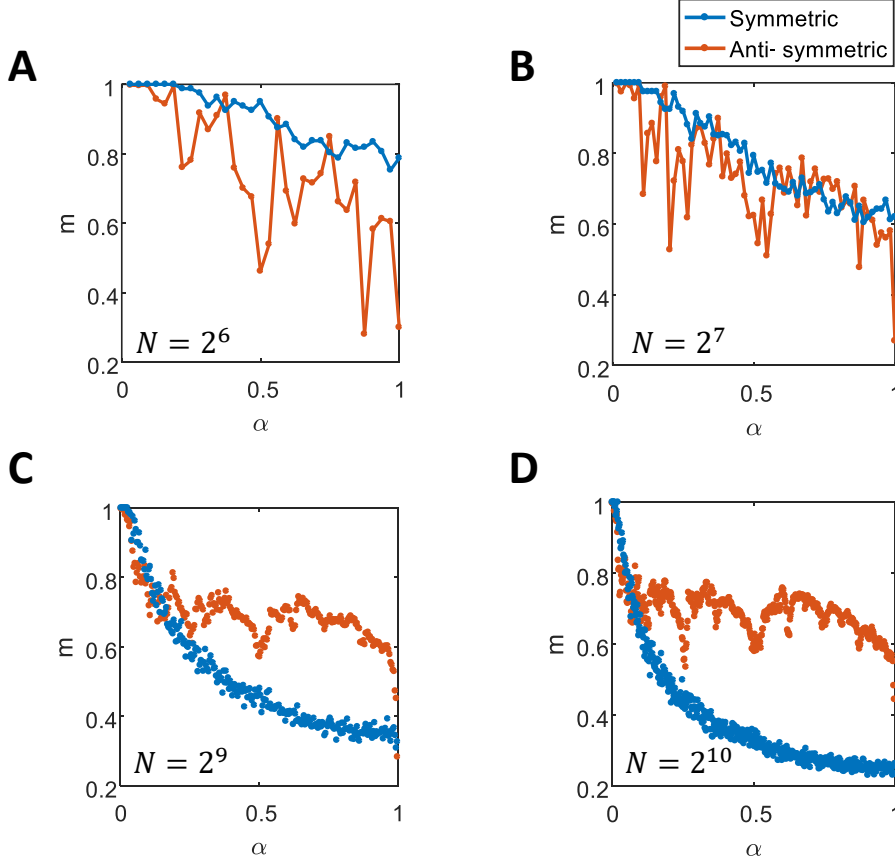


Figure S 5: Capacity of the continuous Hopfield model. Same as in Fig. S5-1, but for the continuous version of the Hopfield model.

S6 Retrieval with volatile connectivity

We analyze the co-evolution of network activity and connectivity during a retrieval event. At the offset of a recall cue, neural dynamics are given by

$$\dot{x} = -x + W\phi(x), \quad (6)$$

and, assuming that the contribution of the learning operator Δ_L is negligible, the synaptic matrix evolves as

$$\dot{W} = \eta_F (\Sigma - \phi\phi^T). \quad (7)$$

Following [40], we write W as a sum of a low-rank structured term and a high-rank random term. In our case, however, the symmetric part of W fluctuates due to the dynamics in Eq. (7). Thus, with one memory plane embedded, connectivity has the form

$$W = \rho (uv^T - vu^T) + \gamma uu^T + \delta vv^T + g\chi, \quad (8)$$

where $\rho > 0$ is constant, γ, δ are time-varying, and $g\chi$ incorporates all eigen-subspaces of W other than the one spanned by u, v . Here we have used the fact that symmetric and anti-symmetric matrices are normal matrices, and thus have orthogonal eigen-decompositions. We assume that the eigen-spaces of χ have small overlap with u, v ; this is not true in general, but is found to be reasonably true numerically, and makes the following calculations easier.

As before, we project \dot{x} from Eq. (6) onto the uv plane, this time yielding (with the notation of S5)

$$\begin{aligned} \dot{p}_u &= -p_u + \rho q_v + \gamma q_u \\ \dot{p}_v &= -p_v - \rho q_u + \delta q_v. \end{aligned}$$

The dynamics of W can similarly be reduced to the relevant dimensions by differentiating Eq. (8) w.r.t time and projecting Eqs. (7,8) onto u, v :

$$\begin{aligned}\dot{\gamma} &= \eta_F (1/2 - q_u^2) \\ \dot{\delta} &= \eta_F (1/2 - q_v^2)\end{aligned}$$

(we have taken here $\Sigma = I/2$ with I the identity matrix on \mathbb{R}^N). The quantity of interest is the real part of the memory eigenvalue, $\lambda_{uv} := \frac{\gamma + \delta}{2}$, which follows the dynamics

$$\dot{\lambda}_{uv} = \frac{\eta_F}{2} (1 - q_u^2 - q_v^2).$$

Denoting the approximation for q derived in S5 by $\tilde{q}_u = \arctan\left(\frac{p_u}{|p_v|}\right)$, and $d := \frac{\gamma - \delta}{2}$ (which is found numerically to be constant up to small fluctuations) retrieval dynamics can be described by the system

$$\begin{aligned}\dot{p}_u &= -p_u + (\lambda_{uv} + d) \tilde{q}_u + \rho \tilde{q}_v \\ \dot{p}_v &= -p_v + (\lambda_{uv} - d) \tilde{q}_v - \rho \tilde{q}_u \\ \dot{\lambda}_{uv} &= \frac{\eta_F}{2} (1 - \tilde{q}_v^2 - \tilde{q}_u^2).\end{aligned}$$

Through this approximation we see how the restraining force ensures homeostasis of neural activity following retrieval: Large overlap with the attractor drives a reduction in λ_{uv} , which in turn makes the limit-cycle less attractive, thus effectively destabilizing it. Once the neural state x is off the uv plane, λ_{uv} is restored to equilibrium values, and the attractor is accessible again.

S7 Model prediction

Our results show that long-term memory retention may arise from orthogonal contributions to network connectivity dynamics. Assuming that the anti-symmetric component of the connectivity matrix W stores memories, our model predicts that during rest this component should be invariant, and only change during learning epochs. Here we show how this prediction may be tested on experimental data.

We assume that we have access to the temporal evolution of effective connectivity weights between pairs of reciprocally connected neurons, during learning and during rest. Given such data, our model predicts that during rest, the changes to reciprocal connections should be highly correlated (Fig. S7A,B; top). During learning, connectivity is modified also by an anti-symmetric Hebbian update, and the above correlation is expected to decrease; this decrease may be very sharp (Fig. S7A, bottom), corresponding to large changes during learning, or may be milder (Fig. S7B, bottom). Considering all possible connection pairs in a memory-encoding network, correlations are close to perfect during pre-learning rest (Fig. S7C, top; blue), and become biased toward anti-correlation during learning (Fig. S7C, top). Following learning, synaptic fluctuations return to be highly correlated, although slightly lower in comparison to pre-learning correlations (Fig. S7C, top; red).

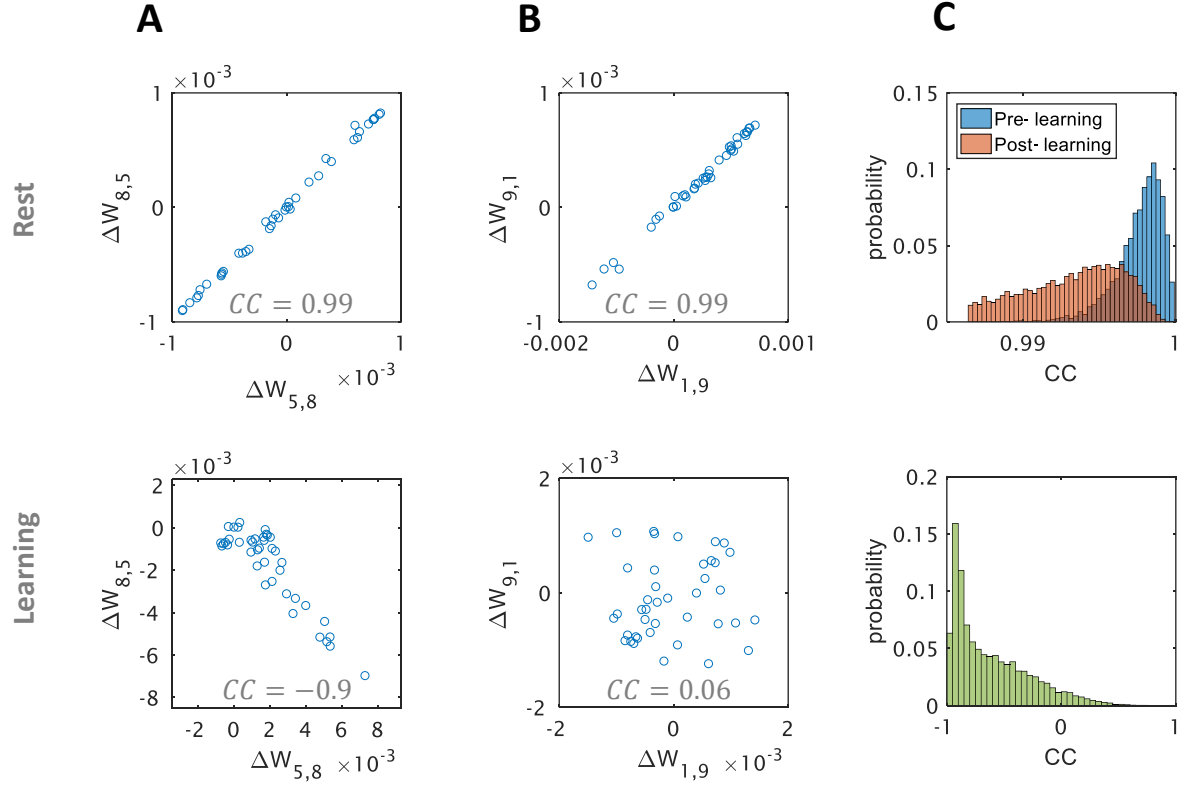


Figure S 7: Assessing model prediction on a numerical simulation. (A,B) Change in W_{ji} as a function of change in W_{ij} during rest (top) and during learning (bottom) for two pairs of reciprocal connections, computed from a single simulation of our model (given by equation (3) in the main text; $N = 128$). Synaptic trajectories are sampled over an interval of 40 time-constants; each circle represents one sampled value. Pearson correlation coefficients (CC) are marked within each panel. (C) Probability distribution of CCs of all cell pairs in the simulated network, during pre- and post-learning rest (top), and during learning (bottom).